Oxidative Addition versus Dehydrogenation of Methane, Silane, and Heavier AH_4 Congeners Reacting with Palladium

Joost N. P. van Stralen and F. Matthias Bickelhaupt*

Afdeling Theoretische Chemie, Scheikundig Laboratorium der Vrije Universiteit, De Boelelaan 1083, NL-1081HV Amsterdam, The Netherlands

Received March 29, 2006

We have computationally studied the oxidative addition of AH_4 to Pd (with A = C, Si, Ge, Sn, and Pb) using relativistic density functional theory (DFT) at ZORA-BLYP/TZ2P. Our purpose is threefold: (i) exploring the occurrence and competition between direct oxidative insertion (OxIn) into the A−H bond and an alternative S_N2-type mechanism that is known to occur for oxidative addition of carbon−halogen bonds; (ii) exploring the trends in activation and reaction enthalpies as the atom A in AH_4 descends in group 14 from carbon to lead; (iii) analyzing and understanding the emerging trends in terms of properties of the reactants using the activation strain model. We find that oxidative insertion of Pd proceeds via a reactant complex and a central barrier only for the C−H bond. For the heavier A−H bonds, the process is barrierless and significantly more exothermic. The higher barrier and smaller exothermicity in the case of Pd + CH_4 has two main reasons: (i) the higher strain associated with the stronger C−H bond and (ii) the weaker Pd−CH_4 interaction due to less attractive electrostatic interaction with the compact and less polar charge distribution of methane. Backside nucleophilic attack proceeds in none of the cases toward an S_N2-type mechanism for oxidative addition. Instead, the process evolves into a novel mechanism for α-elimination of molecular hydrogen.

1. Introduction

Oxidative addition (eq 1) is a key step in many catalytic reactions[1] and has thus been intensively investigated both experimentally[2] and theoretically.[3,4]

$$ML_n + R{-}X \underset{\text{reductive elimination}}{\overset{\text{oxidative addition}}{\rightleftharpoons}} R{-}ML_n{-}X \qquad (1)$$

Previously, we have investigated oxidative addition of C−H, C−C, C−Cl, and C−F bonds to Pd(0).[5−11] One of these model reactions has been the direct oxidative insertion (OxIn) of Pd into the C−H bond of CH_4. In the present study, we extend our previous investigations to the heavier group 14 analogues of methane CH_4, i.e., to silane SiH_4, germane GeH_4, stanane SnH_4, and plumbane PbH_4. Thus, we have explored and analyzed in detail the *intrinsic* reactivity of the uncoordinated Pd atom toward AH_4 (A = Si, Ge, Sn, Pb) using relativistic density functional theory (DFT) at ZORA-BLYP/TZ2P. This approach has been recently shown to agree well with high-level coupled-cluster benchmarks for C−H,[8,9] C−C,[10] and C−F bond activation.[11] Palladium was chosen because this metal is widely used in catalysis[12] and because the atom has a stable closed-shell d^{10} ground state,[4,13] which facilitates comparison with the behavior of closed-shell transition metal complexes used in practice.

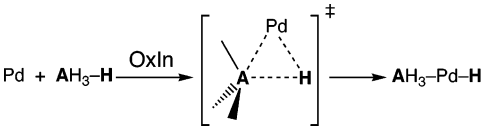

(2)

We aim at three objectives. First, we wish to explore the trends in activation and reaction enthalpies for A−H bond activation through direct oxidative insertion (OxIn) as the atom A in AH_4 descends in group 14 from carbon to lead (eq 2). The η^2-coordination of the heavier AH_4 analogues to metal complexes may serve as a model for methane and alkane coordination with subsequent activation of the C−H bond, which

* To whom correspondence should be addressed. Fax: +31-20-59 87629. E-mail: FM.Bickelhaupt@few.vu.nl.

(1) Elschenbroich, Ch. *Organometallics*; Wiley-VCH: Weinheim, 2006. Collman, J. P.; Hegedus, L. S.; Norton, J. R.; Finke, R. G. *Principles and Applications of Organotransition Metal Chemistry*; University Science Books: Mill Valley, CA, 1987.

(2) Crabtree, R. H. *Chem. Rev.* **1995**, *95*, 987. Crabtree, R. H. *J. Organomet. Chem.* **2004**, *689*, 4083. Shilov, A. E.; Shul'pin, G. B. *Chem. Rev.* **1997**, *97*, 2879. Corey, J. Y.; Braddock-Wilking, J. *Chem. Rev.* **1999**, *99*, 175. van der Boom, M. E.; Milstein, D. *Chem. Rev.* **2003**, *103*, 1759. Weisshaar, J. C. *Acc. Chem. Res.* **1993**, *26*, 213.

(3) Carroll, J. J.; Haug, K. L.; Weisshaar, J. C.; Blomberg, M. R. A.; Siegbahn, P. E. M.; Svensson, M. *J. Phys. Chem.* **1995**, *99*, 13955. Torrent, M.; Solà, M.; Frenking, G. *Chem. Rev.* **2000**, *100*, 439. Griffin, T. R.; Cook, D. B.; Haynes, A.; Pearson, J. M.; Monti, D.; Morris, G. E. *J. Am. Chem. Soc.* **1996**, *118*, 3029. Ziegler, T. *Chem. Rev.* **1991**, *91*, 651. Heiberg, H.; Gropen, O.; Swang, O. *Int. J. Quantum Chem.* **2003**, *92*, 391. Niu, S. Q.; Hall, M. B. *Chem. Rev.* **2000**, *100*, 353. Siegbahn, P. E. M. *J. Am. Chem. Soc.* **1996**, *118*, 1487. Wittborn, A. M. C.; Costas, M.; Blomberg, M. R. A.; Siegbahn, P. E. M. *J. Chem. Phys.* **1997**, *107*, 4318.

(4) Dedieu, A. *Chem. Rev.* **2000**, *100*, 543.

(5) Diefenbach, A.; de Jong, G, Th.; Bickelhaupt, F. M. *J. Chem. Theory Comput.* **2005**, *1*, 286.

(6) Diefenbach, A.; Bickelhaupt, F. M. *J. Chem. Phys.* **2001**, *115*, 4030. Diefenbach, A.; de Jong, G. Th.; Bickelhaupt, F. M. *Mol. Phys.* **2005**, *103*, 995.

(7) Diefenbach, A.; Bickelhaupt, F. M. *J. Phys. Chem. A* **2004**, *108*, 8460.

(8) de Jong, G. Th.; Solà, M.; Visscher, L.; Bickelhaupt, F. M. *J. Chem. Phys.* **2004**, *121*, 9982.

(9) de Jong, G. Th.; Geerke, D. P.; Diefenbach, A.; Bickelhaupt, F. M. *Chem. Phys.* **2005**, *313*, 261.

(10) de Jong, G. Th.; Geerke, D. P.; Diefenbach, A.; Solà, M.; Bickelhaupt, F. M. *J. Comput. Chem.* **2005**, *26*, 1006.

(11) de Jong, G. Th.; Bickelhaupt, F. M. *J. Phys. Chem. A* **2005**, *109*, 9685.

(12) Malleron, J.-L.; Fiaud, J.-C.; Legros, J.-Y. *Handbook of Palladium Catalyzed Organic Reactions*; Academic Press: New York, 1997.

(13) Pyykkö, P. *Chem. Rev.* **1988**, *88*, 563.

10.1021/om060274g CCC: $33.50
Publication on Web 07/21/2006

has also been the subject of experimental studies involving SiH_4, GeH_4, and SnH_4.[14,15] Understanding the factors that determine the trends in the kinetics and thermochemistry of A−H bond activation may shed light on the underlying mechanisms and, in this way, assist a more rational design of transition metal complexes that activate alkane C−H bonds.

A second purpose is the quest for an alternative S_N2-type mechanism for A−H bond activation. Such an S_N2-type mechanism was found to occur for Pd + CH_3Cl.[5,7] Here, Pd performs a backside nucleophilic attack that leads to the expulsion of the Cl^- leaving group. The leaving group migrates either in a concerted manner or in a separate second reaction step toward palladium, leading again to the product for oxidative addition. In the present case, we deal with the H^- leaving group (eq 3).

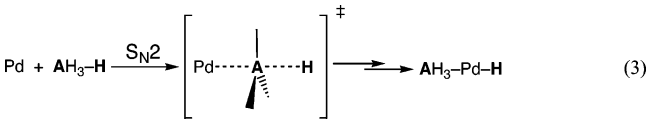

(3)

The hydride anion is a poor leaving group with a significantly higher proton affinity (PA) than the chloride leaving group. Here, we anticipate that this does indeed lead to deviations from the normal S_N2 reaction path, which evolves into palladium-induced 1,1-elimination (1,1-E) of molecular hydrogen via a novel mechanism. We discuss the significance of this reaction channel in the dehydrogenation of alkanes, such as in the reactions of $M^+ + CH_4$ that have been studied experimentally in the gas phase.[16,17] In this context, we compare the novel S_N2-type pathway with the better known stepwise mechanism that proceeds via initial oxidative insertion followed by a hydrogen shift from carbon to the transition metal and, finally, reductive elimination of H_2 (see, for example, ref 18).

Finally, the trends in reactivity and competition between the various mechanisms are analyzed using the activation strain model of chemical reactivity.[5,19] In this model, activation energies $\Delta E^{\ddagger}$ are decomposed into the activation strain $\Delta E^{\ddagger}_{\text{strain}}$ and the stabilizing transition state (TS) interaction $\Delta E^{\ddagger}_{\text{int}}$: $\Delta E^{\ddagger} = \Delta E^{\ddagger}_{\text{strain}} + \Delta E^{\ddagger}_{\text{int}}$. The activation strain $\Delta E^{\ddagger}_{\text{strain}}$ is the strain associated with deforming the reactants from their equilibrium structure to the geometry they adopt in the TS. The TS interaction $\Delta E^{\ddagger}_{\text{int}}$ is the interaction between the deformed reactants when they are brought together to take their positions in the overall TS species. Here, we use the extended activation strain model in which all energy components are monitored *along the reaction coordinate*. A straightforward relationship emerges between trends in reactivity and the strength (through $\Delta E^{\ddagger}_{\text{strain}}$) and electronic structure (through $\Delta E^{\ddagger}_{\text{int}}$) of the A−H bond.

2. Methods

All calculations are based on density functional theory (DFT)[20,21] and have been performed using the Amsterdam Density Functional (ADF) program.[22] MOs were expanded in a large uncontracted set of Slater-type orbitals (STOs).[23] The basis is of triple-ζ quality, augmented with two sets of polarization functions on each atom: 2p and 3d on hydrogen, 3d and 4f on carbon and silicon, 4d and 4f for germanium, 5d and 4f for tin, and 6d and 5f for lead. The palladium atom is represented by a triple-ζ type basis set augmented with 5p and 4f polarization functions. The core shells of carbon (1s), silicon (1s2s2p), germanium (1s2s2p2s3p), tin (1s2s2p2s3p-3d4s4p), lead (1s2s2p2s3p4s4p4d), and palladium (1s2s2p3s3p3d) were treated by the frozen-core approximation.[24] An auxiliary set of s, p, d, f, and g STOs was used to fit the molecular density and to represent the Coulomb and exchange potentials accurately in each SCF cycle.[25]

Geometries and energies were calculated using the generalized gradient approximation (GGA). Exchange is described by Slater's X α potential,[26] with nonlocal corrections due to Becke.[27] Correlation is treated in the Vosko−Wilk−Nusair (VWN) parametrization using formula V,[28] with nonlocal corrections due to Lee, Yang, and Parr.[29] Scalar relativistic effects were taken into account by the zeroth-order regular approximation (ZORA).[30]

All energy minima and transition state[31] structures were verified by frequency calculations:[32] for minima all normal modes have real frequencies, whereas transition states have one normal mode with an imaginary frequency. The character of the normal mode associated with the imaginary frequency was analyzed to ensure that the correct transition state was found. Intrinsic reaction coordinate[33] (IRC) calculations have been performed, and the resulting IRC paths were used to compute and analyze the corresponding potential energy surfaces (PES) in the extended activation strain analyses (see Section 3.2). Bond enthalpies at 298.15 K and 1 atm (ΔH_{298}) were calculated from electronic bond energies (ΔE) and our frequency computations using standard statistical-mechanics relationships for an ideal gas.[34]

(14) Schubert, U. *Adv. Organomet. Chem.* **1990**, *30*, 151. Carlton, L.; Molapisi, J. J. *J. Organomet. Chem.* **2000**, *609*, 60. Bakhtiar, R.; Jacobson, D. B. *Organometallics* **1993**, *12*, 2876.

(15) Luo, X. L.; Kubas, G. J.; Burns, C. J.; Bryan, J. C.; Unkefer, C. J. *J. Am. Chem. Soc.* **1995**, *117*, 1159. Fan, M. F.; Jia, G. C.; Lin, Z. Y. *J. Am. Chem. Soc.* **1996**, *118*, 9915. Vincent, J. L.; Luo, S.; Scott, B. L.; Butcher, R.; Unkefer, C. J.; Burns, C. J.; Kubas, G. J.; Lledos, A.; Maseras, F.; Tomas, J. *Organometallics* **2003**, *22*, 5307.

(16) Pavlov, M.; Blomberg, M. R. A.; Siegbahn, P. E. M.; Wesendrup, R.; Heinemann, C.; Schwarz, H. *J. Phys. Chem. A* **1997**, *101*, 1567.

(17) Eller, K.; Scharz, H. *Chem. Rev.* **1991**, *91*, 1121.

(18) Heinemann, C.; Wesendrup, R.; Schwarz, H. *Chem. Phys. Lett.* **1995**, *239*, 75.

(19) Bickelhaupt, F. M. *J. Comput. Chem.* **1999**, *20*, 114.

(20) Dreizler, R. M.; Gross, E. K. U. *Density Functional Theory: An Approach to the Quantum Many-Body Problem*; Springer: Berlin, 1990. Parr, R. G.; Yang, W. *Density-Functional Theory of Atoms and Molecules*; Oxford University Press: New York, 1989.

(21) Bickelhaupt, F. M.; Baerends, E. J. In *Reviews in Computational Chemistry*; Lipkowitz, K. B., Boyd, D. B., Eds.; Wiley-VCH: New York, 2000; Vol. 15. Baerends, E. J.; Gritsenko, O. V. *J. Phys. Chem. A* **1997**, *101*, 5383.

(22) te Velde, G.; Bickelhaupt, F. M.; Baerends, E. J.; Fonseca Guerra, C.; van Gisbergen, S. J. A.; Snijders, J. G.; Ziegler, T. *J. Comput. Chem.* **2001**, *22*, 932. Fonseca Guerra, C.; Snijders, J. G.; te Velde, G.; Baerends, E. J. *Theor. Chem. Acc.* **1998**, *99*, 391. *SCM*, Theoretical Chemistry, Vrije Universiteit, Amsterdam, The Netherlands, http://www.scm.com.

(23) Snijders, J. G.; Baerends, E. J.; Vernooijs, P. *At. Data Nucl. Data Tables* **1982**, *26*, 483.

(24) Baerends, E. J.; Ellis, D. E.; Ros, P. *Chem. Phys.* **1973**, *2*, 41.

(25) Krijn, J.; Baerends, E. J. *Fit-functions in the HFS-method (Int. Report in Dutch)* **1984**.

(26) Slater, J. C. *Quantum Theory of Molecules and Solids*; McGraw-Hill: New York, 1974.

(27) Becke, A. D. *J. Chem. Phys.* **1986**, *84*, 4524. Becke, A. D. *Phys. Rev. A* **1988**, *38*, 3098.

(28) Vosko, S. H.; Wilk, L.; Nusair, M. *Can. J. Phys.* **1980**, *58*, 1200.

(29) Lee, C. T.; Yang, W. T.; Parr, R. G. *Phys. Rev. B* **1988**, *37*, 785.

(30) Chang, C.; Pélissier, M.; Durand, P. *Phys. Scr.* **1986**, *34*, 394. van Lenthe, E.; Baerends, E. J.; Snijders, J. G. *J. Chem. Phys.* **1993**, *99*, 4597. van Lenthe, E.; Baerends, E. J.; Snijders, J. G. *J. Chem. Phys.* **1994**, *101*, 9783. van Lenthe, E.; van Leeuwen, R.; Baerends, E. J.; Snijders, J. G. *Int. J. Quantum Chem.* **1996**, *57*, 281.

(31) Fan, L.; Ziegler, T. *J. Chem. Phys.* **1990**, *92*, 3645.

(32) Fan, L.; Versluis, L.; Ziegler, T.; Baerends, E. J.; Ravenek, W. *Int. J. Quantum Chem.* **1988**, 173.

(33) Fukui, K. *Acc. Chem. Res.* **1981**, *14*, 363. Deng, L.; Ziegler, T.; Fan, L. *J. Chem. Phys.* **1993**, *99*, 3823.

(34) Atkins, P. W. *Physical Chemistry*; Oxford University Press: Oxford, 1998.

Scheme 1. Reaction Mechanisms and Nomenclature of This Study

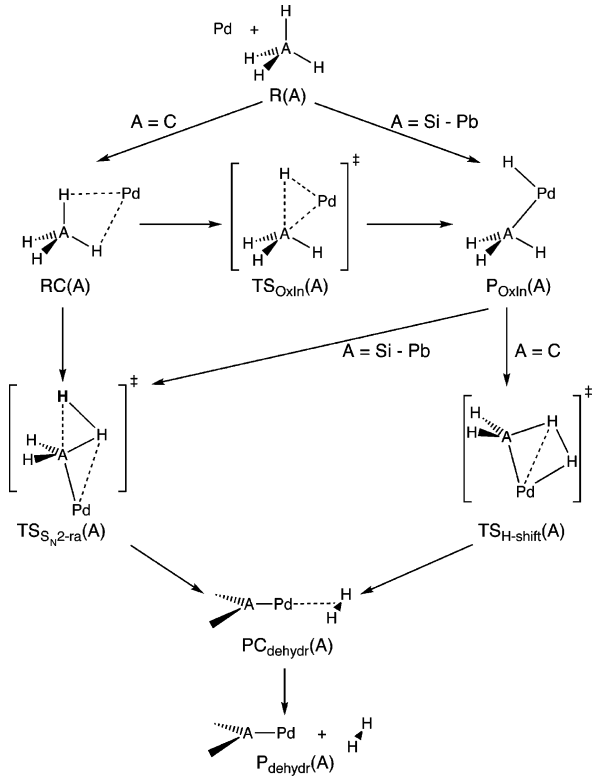

3. Results and Discussion

3.1. Reaction Profiles and Geometries. In this section, we discuss the potential energy surfaces (PES) of our Pd + AH_4 model reactions. Scheme 1 provides an overview of the various mechanisms and illustrates the nomenclature used to designate the stationary points. Our results are summarized in Figures 1 and 2 (geometries) and Tables 1 and 2 (thermochemistry) and in Table S1 (thermochemistry) in the Supporting Information. The trends are analyzed in Section 3.3 in terms of the activation strain model that is presented in Section 3.2.

Direct Oxidative Insertion (OxIn). First, we discuss the direct oxidative insertions (OxIn) of Pd into the A−H bonds (eq 2). Only for the methane C−H bond does the insertion of Pd proceed via a central barrier (see Scheme 1). Insertion into the heavier A−H bonds occurs spontaneously, that is, without a barrier (see Scheme 1). The OxIn reaction of Pd + CH_4 proceeds, via the −7.5 kcal/mol exothermic formation of reactant complex **1b**, toward the transition state **1c** at 0.5 kcal/mol relative to reactants and 8.0 kcal/mol relative to the reactant complex and, finally, to the OxIn product **1d** (all values are 298 K enthalpies, see Table 1). The reaction is exothermic by −6.1 kcal/mol relative to reactants (Table 1). The product (**1d**) is however slightly *less stable* relative to the reactant complex (**1b**). Note that in the reactant complex (**1b**), methane is coordinated to the Pd in an η^2-fashion via two C−H bonds (H,H coordination, see Figure 2). This is relevant in view of the fact that coordination complexes of SiH_4 are used as models for the activation of alkane C−H bonds. They differ however from the latter in that they do not form H,H-η^2 complexes as in **1b** but Si,H-η^2 complexes in which the metal center interacts side-on with one Si−H bond.[15] For more details on the Pd + CH_4 reaction, see earlier investigations.[8,9]

The OxIn reaction barrier disappears as the central atom in AH_4 changes from carbon to one of the heavier group 14 atoms (see Scheme 1). Thus, oxidative insertion of Pd into the Si−H, Ge−H, Sn−H, and Pb−H bonds proceeds spontaneously, without prior formation of a stable reactant complex and without encountering a transition state (see Table 1 and Figure 1). The disappearance of the OxIn barrier from C−H to Si−H is accompanied with a drastic increase in the overall exothermicity of the reaction from −6.1 to −33.1 kcal/mol (see Table 1). Thereafter, the reaction enthalpy changes more moderately from −33.1 (Si−H) to −37.1 (Ge−H) to −45.0 (Sn−H) to −41.0 kcal/mol (Pb−H).[35] Furthermore, as the A−H bond length in the isolated AH_4 substrate increases from 1.095 (C−H, **1a**) to 1.491 (Si−H, **2a**) to 1.537 (Ge−H, **3a**) to 1.723 (Sn−H, **4a**) to 1.785 Å (Pb−H, **5a**), the relative (but also the absolute) elongation of the activated A−H bond in the OxIn product decreases from 126 (C−H, **1d**) to 59 (Si−H, **2d**) to 61 (Ge−H, **3d**) to 44 (Sn−H, **4d**) to 33% (Pb−H, **5d**). The changes from C−H (large stretching in TS) to Si−H (less stretching in TS) are again more pronounced than those along the heavy A−H bonds (see Figures 1 and 2).

The enhanced reactivity of the heavier AH_4 substrates compared to methane agrees nicely with the experimental observation that Ni atoms react spontaneously at 12 K with SiH_4 and SnH_4 to yield the insertion products SiH_3NiH and SnH_3-NiH, respectively.[36] It is, however, not clear in these experiments if the barrier for Ni insertion into the Si−H and Sn−H bonds is completely absent or just very low. On the other hand, again in agreement with our findings for Pd, the Ni atom does *not* spontaneously insert into the C−H bond of CH_4. The insertion product of that reaction is only observed after photochemical activation of the nickel atom.[36]

The barrier-free insertion of uncoordinated Pd into the silane Si−H bond that we find contrasts with the behavior of the Pd-$(PH_3)_2$ complex, which shows a barrier as found by Sakaki et al.[37] The introduction of two phosphine ligands in the latter causes the metal system to form a stable reactant complex with silane prior to going through a transition state for insertion into the Si−H bond. We have previously[38] related the reduced reactivity of Pd after coordinating phosphine ligands to the associated introduction of a catalyst component in the activation strain (see Section 3.2). Thus, as the substrate binds via the A−H bond to the metal center of the $Pd(PH_3)_2$, the phosphine ligands must bend away, giving rise to an increased strain energy in the metal complex. This increased "catalyst activation strain" is one factor that reduces the reactivity of the metal complex compared to the uncoordinated metal atom.

Nucleophilic Attack Leading to Dehydrogenation. We have also explored the possible occurrence of an alternative S_N2 mechanism for oxidative addition of Pd + AH_4 (eq 3). As mentioned in the Introduction, such a mechanism (eq 3) has been found for Pd + CH_3Cl.[5,7] Indeed, for all five model substrates, we do find an alternative reaction channel that is initiated by nucleophilic attack of Pd at the central atom A in AH_4, at the opposite side of the A−H bond that is activated. In early stages, this reaction mechanism closely resembles a regular S_N2 substitution: as the nucleophilic Pd approaches toward the central atom A, the hydride leaving group begins to move away.

(35) Reaction energies (i.e., without enthalpy and zero-point vibrational energy corrections) differ only a few kcal/mol from the enthalpies, but they show a steady, monotonic increase in exothermicity along palladium-induced C−H through Pb−H bond activation.

(36) Himmel, H. J. *Chem. Eur.* **2004**, *10*, 2851.

(37) Sakaki, S.; Ogawa, M.; Kinoshita, M. *J. Phys. Chem.* **1995**, *99*, 9933.

(38) Diefenbach, A.; Bickelhaupt, F. M. *J. Organomet. Chem.* **2005**, *690*, 2191.

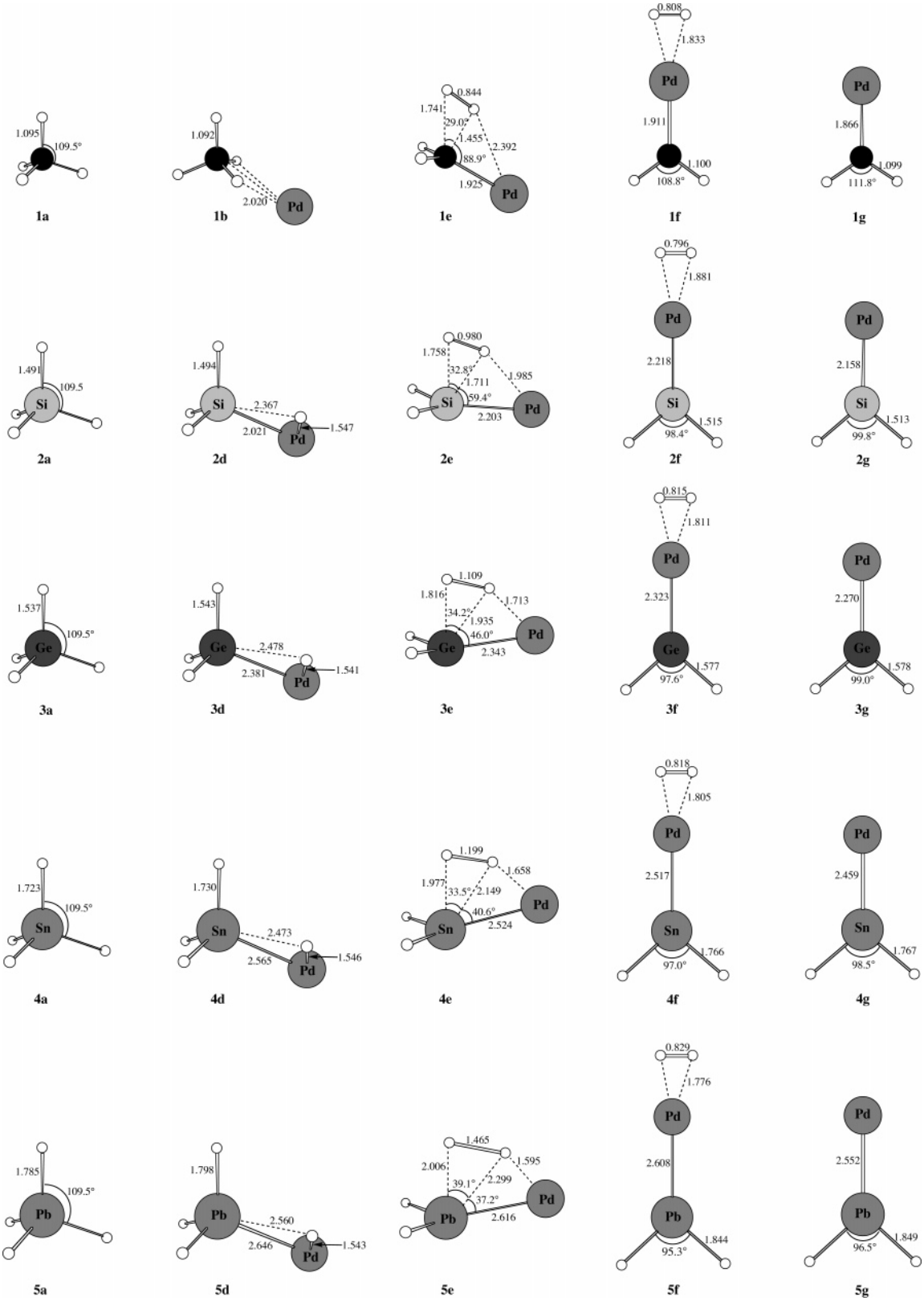

Figure 1. Geometries (in Å, deg) at ZORA-BLYP/TZ2P of stationary points along the potential energy surfaces for oxidative insertion (OxIn) and dehydrogenation of Pd + AH_4 bond with A = C, Si, Ge, Sn, and Pb.

The reaction channel found is also very reminiscent of a metathesis reaction.

There are however a number of striking differences between the present S_N2-type reactions and the one that was found for Pd + CH_3Cl.[5,7] In the first place, while in the case of A = C a regular reactant complex RC(C) exists for Pd + AH_4, there is no such structure for A = Si, Ge, Sn, and Pb from which Pd can nucleophilically attack the backside of an intact substrate AH_4. This is because, as mentioned above, the metal atom inserts spontaneously into the heavier A−H bonds under formation of P_{OxIn}(A) (see Scheme 1). Nevertheless, the system can evolve also from this structure to approach the geometry of an S_N2-

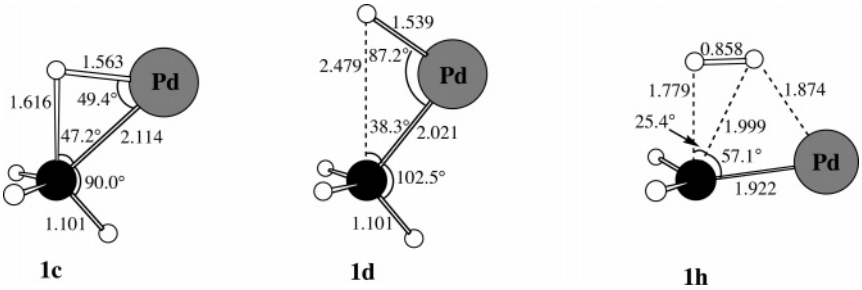

Figure 2. Geometries (in Å, deg) at ZORA-BLYP/TZ2P of the TS_{OxIn}(C) **1c**, P_{OxIn}(C) **1d**, and $TS_{H-shift}$(C) **1h** of Pd + CH_4.

Table 1. Reaction Profiles for Oxidative Insertion (OxIn) and Two Dehydrogenation Reactions (S_N2-ra and H-shift) of Pd + AH4 (A = C, Si, Ge, Sn, and Pb): 298 K Enthalpies (in kcal/mol) Relative to the Reactants[a]

reactants	RC	TS_{OxIn}[b]	P_{OxIn}	TS_{S_N2-ra}	$TS_{H-shift}$	PC_{dehydr}	Pd_{ehydr}
Pd + CH_4	−7.5	0.5 (5.6)	−6.1	46.8 (52.6)	47.0 (52.5)	28.2	38.1
Pd + SiH_4	*c*	*c*	−33.1	−5.5 (0.9)	*d*	−18.5	−12.0
Pd + GeH_4	*c*	*c*	−37.1	−11.8 (−5.5)	*d*	−32.1	−22.6
Pd + SnH_4	*c*	*c*	−45.0	−21.8 (−15.8)	*d*	−45.7	−36.0
Pd + PbH_4	*c*	*c*	−41.0	−23.2 (−16.2)	*d*	−56.5	−44.3

[a] See Scheme 1. Computed at ZORA-BLYP/TZ2P. [b] 298 K Gibbs free energies in parentheses (see also Table S1). [c] Does not exist (OxIn reaction proceeds without barrier). [d] No alternative $TS_{H-shift}$ leading to PC_{dehydr}.

Table 2. Homolytic A−H Bond Dissociation (ΔH_{homo}) and Dehydrogenation Enthalpies Leading to Singlet (ΔH_{dehydr}(s)) and Triplet AH_2 (ΔH_{dehydr}(t)) (A = C, Si, Ge, Sn, and Pb)[a]

AH_4	ΔH_{homo}	ΔH_{dehydr}(s)	ΔH_{dehydr}(t)
CH_4	102.2	118.9	108.9
SiH_4	87.8	50.2	73.1
GeH_4	77.4	27.0	56.8
SnH_4	66.9	8.0	38.6
PbH_4	56.8	−16.8	21.8

[a] Computed for 298 K at ZORA-BLYP/TZ2P. See also eqs 5 and 6 and Tables S2 and S3.

type transition state in which the Pd atom approaches the central atom A while the H atom on the other side begins to leave.

Interestingly, however, as the reaction proceeds, the nature of our reaction channel begins to differ qualitatively from a normal S_N2 mechanism. It yields neither the product complex of an S_N2 reaction nor a configuration rearranged to the oxidative-addition product (as found for Pd + CH_3Cl)[5,7] in which the leaving group has migrated around the substrate and eventually coordinates to Pd, i.e., [Pd-AH_3^+, H^-] and AH_3−Pd−H, respectively. Instead, we find palladium-induced dehydrogenation (or 1,1-elimination) of the substrate (eq 4): What

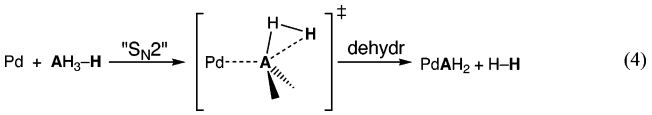

(4)

happens is that the hydride leaving group is a sufficiently strong base to abstract, in concert with its leaving the central atom, a proton from the AH_3 cation that is coordinated to Pd (eq 4). This results in the formation of product complex [Pd(AH_2)(H_2)], in which H_2 binds weakly, i.e., by roughly 10 kcal/mol, to Pd (see Table 1). Eventually, $PdAH_2$ + H_2 are formed (eq 4). The present dehydrogenation via 1,1-elimination is reminiscent of the hydrogen fluoride elimination that occurs in the S_N2-type mechanism of Pd + CH_3F.[11]

The reaction proceeds in all cases via the same type of transition state, TS_{S_N2-ra}(A), shown schematically in eq 4 and Scheme 1 and in scale in Figure 1. There is again a sharp demarcation between the reactions of methane and those of its heavier analogues. The S_N2-type dehydrogenation pathway of Pd + CH_4 proceeds via the same reactant complex (**1b**) as the OxIn reaction, but, thereafter, it goes through a high-energy TS_{S_N2-ra} (**1e**) that is 46.8 kcal/mol above the reactants (see Table 1). In this TS_{S_N2-ra} (**1e**), the C−H bond with the hydrogen acting as leaving group has been stretched by 0.646 Å (59%) and amounts to 1.741 Å (see Figure 1). This leaving-group H is binding to another H atom (H−H = 0.844 Å; compare this with 0.746 Å in free H_2) that is in the process of being abstracted, having a relatively long A−H distance of 1.455 Å. This latter H atom is still distant from palladium, with a H−Pd distance of 2.392 Å (H−Pd = 1.833 Å in the product complex PC_{dehydr}(C) **1f**, see Figure 1). Overall, H_2 elimination from methane is highly endothermic, with a reaction enthalpy of +38.1 kcal/mol (see Table 1). On the other hand, if one goes to the heavier AH_4 analogues, the enthalpy of the TS_{S_N2-ra}(A) (**2e**−**5e**) drops below that of the reactants with values that range from −5.5 (SiH_4) to −23.2 kcal/mol (PbH_4); see Table 1. Accordingly, the TS_{S_N2-ra}(A) becomes more "educt-like" in the sense that both the absolute and relative stretching of the leaving-group A−H bond decreases further monotonically from 0.267 Å, or 18% (SiH_4, **2e**), to 0.221 Å, or 12% (PbH_4, **5e**); see Figure 1. Note also that along this series the extent of H−H bond formation in the transition state decreases (i.e., the H−H distance increases) and the agostic assistance by Pd becomes more pronounced (i.e, the Pd−H distance becomes shorter); see Figure 1. In line with the decreasing barriers, the reaction becomes exothermic with heats of reaction ranging from −12.0 (SiH_4) to −44.3 kcal/mol (PbH_4); see Table 1.

The dehydrogenation pathway of Pd + AH_4, that is, the formation of $PdAH_2$ + H_2, is less exothermic than oxidative insertion, that is, the formation of AH_3PdH for A = C, Si, Ge, and Sn, but for A = Pb, dehydrogenation is *more* exothermic than insertion: compare P_{dehydr} with P_{OxIn} in Table 1 (if one compares the *product complex* PC_{dehydr} with P_{OxIn}, the dehydrogenation pathway becomes more exothermic than insertion already for A = Sn and is so *by more than 15 kcal/mol* for A = Pb). This trend of increasing relative stability of the dehydrogenation pathway is largely determined by the trend in relative stabilities of the carbene-type AH_2 species and $AH_3^{\bullet}$

radicals. In Table 2, we have compared the reaction enthalpies for homolytic A−H bond dissociation (eq 5) and H_2 elimination (eq 6) from AH_4 (see Table 2).

$$AH_4 \rightarrow AH_3^{\bullet} + H^{\bullet} \quad (5)$$

$$AH_4 \rightarrow AH_2 + H_2 \quad (6)$$

The A−H bond dissociation enthalpy ΔH_{homo} decreases monotonically from 102.2 (CH_4) to 56.8 kcal/mol (PbH_4); see Table 2. This trend is even more pronounced for dehydrogenation of AH_4 in which two A−H bonds are dissociated. Thus, the dehydrogenation enthalpy decreases even more steeply from 108.9 kcal/mol for CH_4 (which preferentially forms triplet carbene) to −16.8 kcal/mol for PbH_4 (all heavier AH_4 lead preferentially to singlet AH_2); see ΔH_{homo}(s) and ΔH_{homo}(t) in Table 2. The fact that $PbH_2 + H_2$ is more stable than PbH_4 has been traced to a (scalar) relativistic effect.[39] We have confirmed that indeed the reaction *energy* ΔE_{dehydr} for conversion of PbH_4 into PbH_2(s) + H_2 is only exothermic (−15.4 kcal/mol) if relativistic effects are taken into account at ZORA-BLYP/TZ2P. It becomes endothermic (+8.0 kcal/mol) if relativistic effects are neglected at BLYP/TZ2P.

Dehydrogenation via Oxidative Insertion. We are primarily interested in C−H and A−H bond activation through OxIn or S_N2 pathways (see Introduction). Nevertheless, the unexpected finding of the novel AH_4 dehydrogenation mechanism described above prompted us to include for comparison the alternative and well-known stepwise mechanism for dehydrogenation, which has been previously invoked in experimental[40] and theoretical[16,18,41] studies on the dehydrogenation (and other pathways) of methane by transition metal cations M^+. This better known mechanism proceeds via initial oxidative insertion, followed by migration of a second hydrogen from A to the transition metal and, finally, reductive elimination of H_2.

Indeed, we find such a mechanism, but only for Pd + CH_4. However, as shown in Scheme 1, it differs from the mechanism found for Pt^+ in that it proceeds, after oxidative insertion, via only one additional transition state, $TS_{H-shift}$(C), which directly leads to the product complex PC_{dehydr}(C), without prior formation of a dihydride intermediate [Pd(AH_2)(H)(H)]. The geometrical nature of $TS_{H-shift}$(C) (**1h**) differs from that of TS_{S_N2-ra}(C) (**1e**) with the evolving H_2 being much closer to Pd in the former than in the latter (see Figures 1 and S1). We have verified through IRC calculations that the two transition states correctly connect the two different pairs of intermediates: $TS_{H-shift}$(C) connects P_{OxIn} with PC_{dehydr}, whereas TS_{S_N2-ra}(C) connects RC with PC_{dehydr}. Interestingly, the overall barrier of 47.0 kcal/mol in the dehydrogenation of methane via $TS_{H-shift}$(C) is slightly higher than that of our novel dehydrogenation mechanism, proceeding via TS_{S_N2-ra}(C) at 46.8 kcal/mol (see Table 1). This suggests that transition metal-induced dehydrogenation of alkanes in the gas phase may also in other cases occur via our novel S_N2-type mechanism.

At this point, we wish to stress that our designation "S_N2-ra" for the dehydrogenation pathway of Pd + SiH_4 and the heavier congeners (vide supra) should not be overrated. This designation is done on the basis of the geometrical nature of the only TS for dehydrogenation of these Pd + AH_4 reaction systems, which more or less resembles that of TS_{S_N2-ra}(C) and less so $TS_{H-shift}$(C) for Pd + CH_4. In TS_{S_N2-ra}(C) (**1e**), the A−H("leaving group") bond breaking is ahead of the stretch in the second A−H bond that must be broken, and the shortest H−Pd distance is significantly longer than in the product of oxidative insertion P_{OxIn}(C) (see Figure 1). In $TS_{H-shift}$(C) (**1h**), it is the other way around: the A−H("leaving group") bond breaking lags behind the stretch in the second A−H bond that must be broken, which in addition has a H−Pd distance that is only somewhat longer than in the product of oxidative insertion P_{OxIn}(C) (see Figure 2). Note that TS_{S_N2-ra}(Si) (**2e**) for dehydrogenation of SiH_4 perfectly resembles TS_{S_N2-ra}(C) (**1e**). But, along GeH_4, SnH_4, and PbH_4 the resemblance of TS_{S_N2-ra}(A) with TS_{S_N2-ra}(C) decreases and that with TSH-shift(C) (**1e**) increases (see Figures 1 and 2). In fact, what happens as we go from A = C to Si is a merging on the PES of the two saddle points TS_{S_N2-ra}(A) and $TS_{H-shift}$(A). Our designation S_N2-ra for the dehydrogenation mechanism for Pb + SiH_4, GeH_4, SnH_4, PbH_4 is therefore not an exact categorization. It rather serves as a reasonable choice of nomenclature to discuss the process.

Finally, the OxIn product can undergo an automerization reaction in which the hydride ligand at palladium is exchanged with a hydrogen of the AH_4 moiety. The shape of the C_{2v}-symmetric TS and the nature of the normal mode (see arrows) are schematically depicted below:

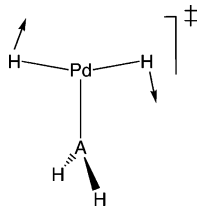

The barrier relative to reactants associated with this TS amounts to 36.7 (C), −7.4 (Si), −15.5 (Ge), −28.7 (Sn), and −34.0 kcal/mol (Pb) (values not shown in Table 1) and is thus always lower than the barrier for subsequent dehydrogenation either via TS_{S_N2-ra} or $TS_{H-shift}$ (see Table 1).

Entropy Effects. Entropy effects at 298 K are important in the sense that they increase the magnitude of the activation free energy $\Delta G^{\ddagger}$ by a few kcal/mol, but they do not discriminate much between the various model reactions and mechanisms considered (see Table 1). Thus, the 298 K activation entropies $\Delta S^{\ddagger}$ are all negative and amount to −17.1 cal/mol K for the oxidative insertion of Pd in methane, −19.6 to −23.8 cal/mol K for the S_N2-type dehydrogenation mechanisms of Pd + AH4, and −18.3 cal/mol K for the dehydrogenation of Pd + CH_4 via 1,2-H shift occurring after initial OxIn (see Table S1). The corresponding $-T\Delta S^{\ddagger}$ values are 5.1 (OxIn of Pd + CH_4) to 7.1 (S_N2-type dehydrogenation of Pd + PbH_4) kcal/mol (see Table S1), which, in terms of relative activation free energies $\Delta G^{\ddagger}$, does essentially not change the picture that arises from the activation enthalpies $\Delta H^{\ddagger}$ (see Table 1) or energies $\Delta E^{\ddagger}$ (vide infra). Therefore, in the following, we focus on further analyzing the origin of and difference between the energy barriers $\Delta E^{\ddagger}$ of the reactions.

3.2. Energy Profiles and the Activation Strain Model. To gain insight into how the activation barriers of the different reactions arise, i.e., insight into how they depend on the nature of the concomitant geometrical deformation and electronic structure of catalyst and substrate, they were analyzed using the activation strain model of chemical reactivity.[7,19,42] In this

(39) Dyall, K. G. *J. Chem. Phys.* **1992**, *96*, 1210.
(40) Irikura, K. K.; Beauchamp, J. L. *J. Am. Chem. Soc.* **1991**, *113*, 2769. Irikura, K. K.; Beauchamp, J. L. *J. Phys. Chem.* **1991**, *95*, 8344.
(41) Perry, J. K.; Ohanessian, G.; Goddard, W. A. *Organometallics* **1994**, *13*, 1870.
(42) Bickelhaupt, F. M.; Baerends, E. J.; Nibbering, N. M. M. *Chem. Eur. J.* **1996**, *2*, 196.

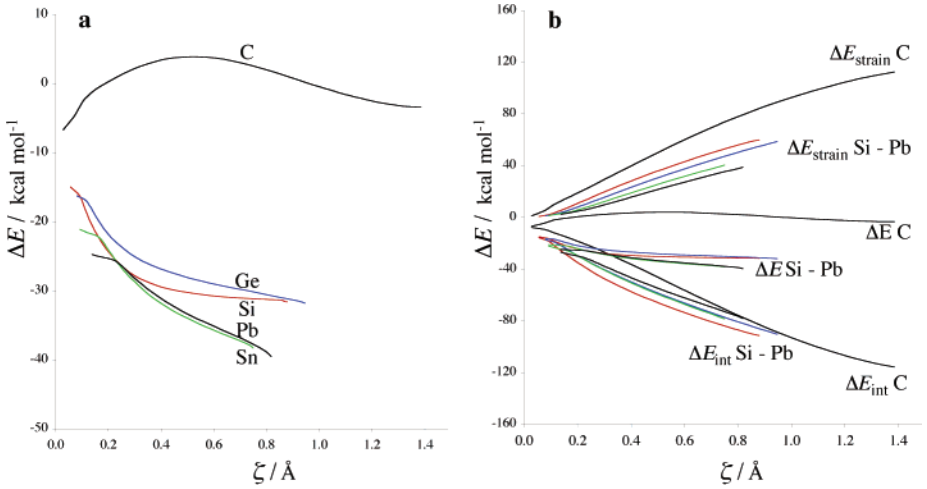

Figure 3. Activation strain analysis along the reaction coordinate of the oxidative insertion (OxIn) of Pd + AH_4 with A = C, Si, Ge, Sn, and Pb: (a) potential energy profiles, $\Delta E(\zeta)$, and (b) their decomposition, $\Delta E(\zeta) = \Delta E_{strain}(\zeta) + \Delta E_{int}(\zeta)$.

model, the activation energy $\Delta E^{\ddagger}$ is decomposed into the activation strain $\Delta E^{\ddagger}_{strain}$ and the transition state (TS) interaction $\Delta E^{\ddagger}_{int}$ (see eq 7):

$$\Delta E^{\ddagger} = \Delta E^{\ddagger}_{strain} + \Delta E^{\ddagger}_{int} \quad (7)$$

The activation strain $\Delta E^{\ddagger}_{strain}$ is the strain energy associated with deforming the reactants from their equilibrium geometry to the geometry they acquire in the activated complex. The TS interaction $\Delta E^{\ddagger}_{int}$ is the actual interaction energy between the deformed reactants in the transition state.

In the present work, we use an extension of the activation strain model: the decomposition of the energy $\Delta E^{\ddagger}(\zeta)$ of the reaction system into strain $\Delta E_{strain}(\zeta)$ of and interaction $\Delta E_{int}(\zeta)$ between the reactants is now carried out along the entire reaction coordinate ζ, i.e., from reactants (or reactant complex) to product (or product complex). This enables us to also investigate why oxidative insertion of Pd into the C−H bonds proceeds via a central barrier with a TS (first-order saddle point), whereas such a barrier is absent for the heavier A−H bonds. The reaction coordinate is determined through IRC computations. In the case of Pd + CH_4, the IRC computations start from the TS_{OxIn}(C) (see **1c** in Figures 2) and lead to the reactant complex **1b** (Figure 1) and the product **1d** (Figure 2). In the case of the heavier AH_4 substrates, the oxidative insertion proceeds barrier-free; that is, there is no TS_{OxIn}(A) from which the IRC computations can start. In these cases, the IRC computations were started from an artificial reactant complex in which Pd coordinates end-on to an A−H bond, yielding a C_{3v}-symmetric species (see Figure S1). This species is a second-order saddle point with two degenerate imaginary frequencies, both corresponding to a mode that leads to the product P_{OxIn} (see **2d**−**5d** in Figure 1). In addition to the OxIn reactions (eq 2), we also subjected the novel S_N2-type dehydrogenation mechanism of Pd + AH_4 to such an extended activation strain analyses along the reaction coordinate.

The TS interaction $\Delta E^{\ddagger}_{int}$ between the strained reactants is further analyzed in the conceptual framework provided by the Kohn−Sham molecular orbital (KS-MO) model[21] (for the OxIn pathways of the heavier AH_4, which proceed without encountering a TS_{OxIn}(A), we have chosen for this bonding energy decomposition the point along the reaction coordinate at which the A−H stretch is equal to the C−H stretch in TS_{OxIn}(C) (**1c**) of Pd + CH_4). Thus, $\Delta E^{\ddagger}_{int}$ is further decomposed into three physically meaningful terms (eq 8) using a quantitative energy decomposition scheme developed by Ziegler and Rauk.[43,44]

$$\Delta E^{\ddagger}_{int} = \Delta V_{elst} + \Delta E_{Pauli} + \Delta E_{oi} \quad (8)$$

The term ΔV_{elst} corresponds to the classical electrostatic interaction between the unperturbed charge distributions of the deformed reactants and is usually attractive. The Pauli repulsion ΔE_{Pauli} comprises the destabilizing interactions between occupied orbitals and is responsible for the steric repulsion. The orbital interaction ΔE_{oi} accounts for charge transfer (interaction between occupied orbitals on one moiety with unoccupied orbitals of the other, including the HOMO−LUMO interactions) and polarization (empty−occupied orbital mixing on one fragment due to the presence of another fragment).

3.3. Analysis of the Energy Profiles and Activation Barriers for Bond Activation. Direct Oxidative Insertion (OxIn). The energy profiles $\Delta E(\zeta)$ of the OxIn reactions of Pd + AH_4 are shown in Figure 3a with the stretch of the activated A−H bond (relative to isolated AH_4) as the reaction coordinate ζ. The figure shows how oxidative insertion of Pd + CH_4 proceeds from RC(C) (**1b**) via a barrier, TS_{OxIn}(C) (**1c**), to the product P_{OxIn}(C) (**1d**), while the OxIn reactions of the heavier AH_4 occur barrier-free to the product P_{OxIn}(A) with A = Si, Ge, Sn, and Pb. In Figure 3b, we show the extended activation strain analysis in which the net energy of the reaction system $\Delta E(\zeta)$ is decomposed into the strain energy $\Delta E(\zeta)_{strain}$ of the substrate AH_4 (the bundle of five upper curves) plus the interaction energy $\Delta E(\zeta)_{int}$ between Pd and AH_4 (the bundle of five lower curves). Not all the details of the energy curves are visible on the scale of Figure 3b. But the two essential effects causing the energy profile $\Delta E(\zeta)$ of Pd + CH_4 to proceed via a barrier are clear: (i) the strain energy $\Delta E(\zeta)_{strain}$ for the reaction of methane is much higher than that of all other AH_4, which show smaller mutual differences; (ii) the Pd−substrate of Pd + CH_4 interaction $\Delta E(\zeta)_{int}$ is less stabilizing than that of all other AH_4, in particular in the early stages of the reactions.

The higher-energy strain curve $\Delta E(\zeta)_{strain}$ for methane is the direct consequence of the well-known fact that the C−H bond is stronger than the Si−H bond. To illustrate this, we compare the A−H bond dissociation enthalpies (eq 5) computed at

(43) Ziegler, T.; Rauk, A. *Theor. Chim. Acta* **1977**, *46*, 1.
(44) Bickelhaupt, F. M.; van Hommes, N. J. R.; Fonseca Guerra, C.; Baerends, E. J. *Organometallics* **1996**, *15*, 2923. Fonseca Guerra, C.; Handgraaf, J. W.; Baerends, E. J.; Bickelhaupt, F. M. *J. Comput. Chem.* **2004**, *25*, 189.

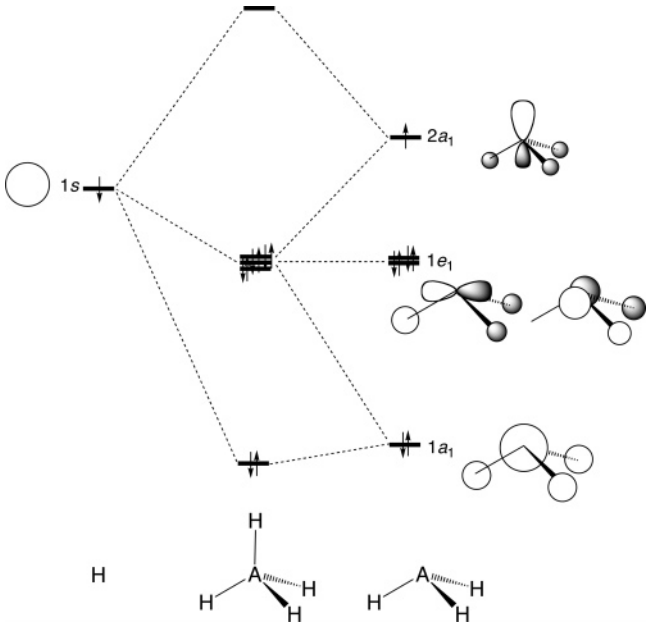

Figure 4. Schematic representation of the valence orbitals of AH_4 arising from the interaction between H• and AH_3• (A = C, Si, Ge, Sn, Pb).

Table 3. Activation Strain Analysis of the Oxidative Insertion (OxIn) of Pd + AH_4 (A = C, Si, Ge, Sn, and Pb)[a]

	CH_4	SiH_4	GeH_4	SnH_4	PbH_4
Energy Decomposition (in kcal/mol)					
$\Delta E^{\ddagger}$	3.9	−30.5	−31.0	−38.1	−40.8
$\Delta E^{\ddagger}_{strain}$	52.2	38.8	37.3	31.3	29.5
$\Delta E^{\ddagger}_{int}$	−48.3	−69.3	−68.2	−69.3	−70.3
ΔE_{Pauli}	201.8	213.0	217.0	205.5	197.3
ΔV_{elst}	−159.2	−191.0	−194.5	−190.4	−181.1
ΔE_{oi}	−90.9	−91.3	−90.8	−84.5	−86.5
VDD Atomic Charges in AH_4 Fragment[b]					
A	−0.031	+0.326	+0.302	+0.360	+0.329
H[c]	−0.014	−0.114	−0.120	−0.144	−0.144

[a] Computed at ZORA-BLYP/TZ2P. For Si, Ge, Sn, and Pb, the point along the energy profile that corresponds to the same A−H stretching as CH_4 experiences is chosen. [b] Voronoi deformation density (VDD) atomic charges; see ref 44. [c] H atom of the activated A−H bond.

ZORA-BLYP/TZ2P: they decrease monotonically from 102 (C−H) to 88 (Si−H) to 77 (Ge−H) to 67 (Sn−H) to 57 kcal/mol (Pb−H). The reason for this is the decreasing bond overlap between the hydrogen 1s AO with the, along this series, still more diffuse AH_3 $2a_1$ singly occupied molecular orbital (SOMO) and the concomitant reduction in stabilization of the bonding $1s + 2a_1$ combination in AH_4 (see Figure 4). The less stabilizing Pd−methane interaction $\Delta E(\zeta)_{int}$ is mainly due to the weaker electrostatic interaction ΔV_{elstat} between Pd and the more compact carbon-based CH_4 molecular orbitals and also because of the less polar character of the C−H compared to the heavier A−H bonds (see Table 3). This follows from the energy decomposition of the Pd−methane TS interaction $\Delta E^{\ddagger}_{int}$ in the TS_{OxIn}(C), which is compared in Table 3 with the decomposition of the Pd−substrate interaction at the point along the reaction coordinate at which the A−H stretch is equal to the C−H stretch in TS_{OxIn}(C) (**1c**) of Pd + CH_4.

Nucleophilic Attack Leading to Dehydrogenation. The results of the activation strain analysis of the S_N2-type pathway leading to dehydrogenation as well as the decomposition of the TS interaction $\Delta E^{\ddagger}_{int}$ are collected in Table 4. They suggest that the main source of the much higher barrier for dehydrogenation of methane is the much higher activation strain, which

Table 4. Activation Strain Analysis of the Dehydrogenation Reaction of Pd + AH_4 (A = C, Si, Ge, Sn, and Pb)[a]

	CH4	SiH4	GeH4	SnH4	PbH4
Energy Decomposition (in kcal/mol)					
$\Delta E^{\ddagger}$	52.6	−2.3	−4.1	−13.0	−21.6
$\Delta E^{\ddagger}_{strain}$	104.2	55.4	52.5	50.5	47.1
$\Delta E^{\ddagger}_{int}$	−51.6	−57.7	−56.6	−63.5	−68.6
ΔE_{Pauli}	222.4	213.2	190.9	184.0	176.2
ΔV_{elst}	−186.0	−195.6	−167.2	−164.9	−153.7
ΔE_{oi}	−87.9	−75.3	−80.3	−82.6	−91.1
VDD Atomic Charges in AH_4 Fragment[b]					
A	−0.089	+0.110	+0.096	+0.123	+0.144
H[c]	+0.052	+0.017	−0.004	−0.012	−0.054
H[d]	+0.047	+0.061	+0.075	+0.066	+0.055

[a] Computed at ZORA BLYP/TZ2P. [b] Voronoi deformation density (VDD) atomic charges; see ref 44. [c] H atom of the activated A−H bond, i.e., the A−H("leaving group") bond. [d] H atom closest to Pd (see **1e**−**5e** in Figure 1).

amounts to 104 kcal/mol compared to 47−55 kcal/mol for the heavier substrates. The TS interaction $\Delta E^{\ddagger}_{int}$ is also less favorable for Pd + CH_4, but the differences are not that much pronounced (see Table 4). There is in fact also not a clear trend in the repulsive and bonding components (ΔE_{Pauli}, ΔV_{elstat}, and ΔE_{oi}) of the TS interaction along the various substrates.

An extended activation strain analysis, along the reaction coordinate, confirms the above picture and also sheds some extra light on the origin of the trend in activation strain (i.e., the sharp decrease from methane to silane) and the absence of a pronounced trend in TS interaction. The energy profiles $\Delta E(\zeta)$ of the S_N2-type dehydrogenation reactions of Pd + AH_4 are shown in Figure 5a with the stretch of the activated A−H("leaving group") bond (relative to isolated AH_4) as the reaction coordinate ζ. The figure shows how all reactions proceed via a barrier, TS_{S_N2-ra}(A), to a situation in which an intact H_2 molecule has been formed. The IRC computation drives aground on an extremely shallow part of the PES just before the pronounced product well of PC_{dehydr} is reached. It is also clear from Figure 5a that the barrier for Pd + CH_4 is much higher than for all other reaction systems.

The more interesting information is contained in Figure 5b. It shows the results of the extended activation strain analysis in which the net energy of the reaction system $\Delta E(\zeta)$ is decomposed into the strain energy $\Delta E(\zeta)_{strain}$ of the substrate AH_4 plus the interaction energy $\Delta E(\zeta)_{int}$ between Pd and AH_4. Not all the details of the energy curves are visible on the scale of Figure 5b, which is even a bit more messy than Figure 3a. But, again, the essential effects causing the energy profile $\Delta E(\zeta)$ of Pd + CH_4 to proceed via a significantly higher barrier (and to be significantly more endothermic) become very clear: (i) the strain energy $\Delta E(\zeta)_{strain}$ for the reaction of methane is much higher than that of all other AH_4, which show smaller mutual differences; (ii) the strain energy $\Delta E(\zeta)_{strain}$ for the reaction of methane increases monotonically, while that of all other AH_4 increases at first much more steeply but then, actually before reaching the TS_{S_N2-ra}(A), goes through a maximum and afterward decreases; and (iii) the Pd−substrate interaction $\Delta E(\zeta)_{int}$ of Pd + CH_4 becomes more stabilizing along the reaction coordinate, while that of Pd + the heavier AH_4 becomes *less* stabilizing and does still so in the region around the transition state TS_{S_N2-ra}(A).

The first two issues (i and ii) are related to both the different starting points in this reaction step for methane (from RC_{OxIn}(C), **1b**) and the heavier substrates (from P_{OxIn}(A), **2b**−**5b**) as well as the much stronger C−H bond (vide supra). The former causes the strain $\Delta E(\zeta)_{strain}$ to already start at a higher energy

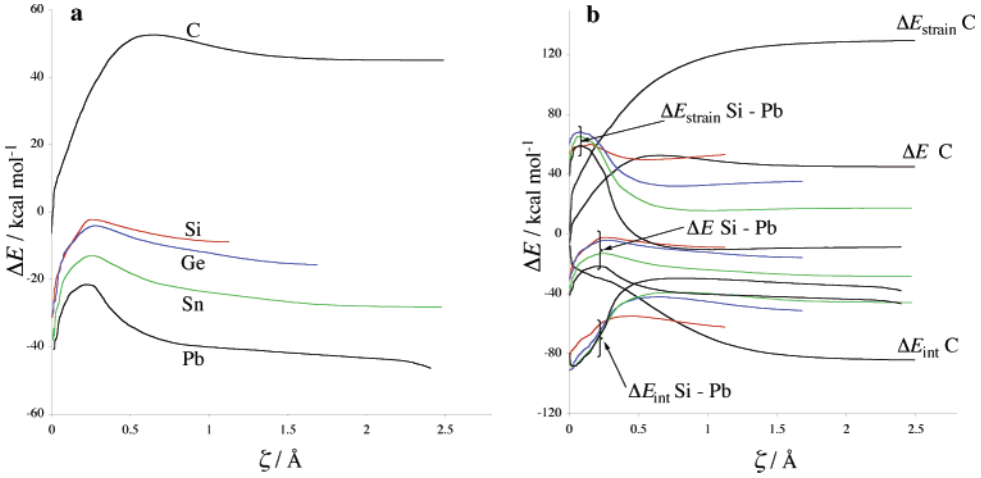

Figure 5. Activation strain analysis along the reaction coordinate of the dehydrogenation of Pd + AH_4 with A = C, Si, Ge, Sn, and Pb: (a) potential energy profiles, $\Delta E(\zeta)$, and (b) their decomposition, $\Delta E(\zeta) = \Delta E_{strain}(\zeta) + \Delta E_{int}(\zeta)$.

because effectively, in P_{OxIn}(A), one A−H bond is already broken, while in RC_{OxIn}(C), no C−H bond is broken. The latter translates into an even larger *difference* in stability between CH_2 and the heavier AH_2, which are about 60 (SiH_2) to 135 kcal/mol (PbH_2) more stable (see Table 2). Thus, after an initial increase of the strain, the formation of the H−H bond can cause the $\Delta E(\zeta)_{strain}$ curve of the heavier substrates to go down again, i.e., to become more stable (see Figure 5b). It can however not turn the trend in the case of methane, resulting in the monotonic increase in strain along the reaction coordinate.

The third issue (iii), i.e., opposite trends in $\Delta E(\zeta)_{int}$ for methane and the heavier substrates, is again related to the different starting points in this reaction step, namely, RC_{OxIn}(C) (**1b**) for the former and P_{OxIn}(A) (**2d**−**5d**) for the latter. The TS interaction $\Delta E(\zeta)_{int}$ of Pd with methane becomes more stabilizing as this initially (in RC_{OxIn}(C)) intact molecule gets more and more deformed. On the other hand, the TS interaction $\Delta E(\zeta)_{int}$ of Pd with the heavier AH_4 is from the outset (in P_{OxIn}(A)) relatively stabilizing and becomes only less stabilizing as we approach the situation with a relatively poorly ligating molecular hydrogen ligand in PC_{dehydr}(A). This also implies that the $\Delta E(\zeta)_{int}$ curves of methane and those of the heavier substrates approach each other as the reaction proceeds toward the transition state. However, the relatively great similarity in TS interaction values $\Delta E^{\ddagger}_{int}$ in Table 4 is probably a matter of coincidence.

4. Conclusions

Methane, silane, and the heavier AH_4 congeners react with palladium preferentially via oxidative insertion into the A−H bond, as follows from our theoretical investigation at ZORA-BLYP/TZ2P. The reaction proceeds for methane via a small barrier, while the process is barrierless and significantly more exothermic for silane and the heavier AH_4 substrates. Using the activation strain model of chemical reactivity, we have traced the higher barrier and smaller exothermicity in the case of Pd + CH_4 to two main factors: (i) the higher strain associated with the stronger C−H bond and (ii) the weaker Pd−CH_4 interaction due to less attractive electrostatic interaction with the compact and less polar charge distribution of methane.

Interestingly, and in contrast to previous findings for chloromethane, backside nucleophilic attack of Pd + CH_4 does not yield an alternative S_N2-type mechanism for oxidative addition in which the leaving group (here: H^-) migrates around the CH_3 moiety toward Pd. Instead, the process evolves into a novel mechanism for α-elimination of molecular hydrogen in which the H^- leaving group abstracts a proton from CH_3. This dehydrogenation pathway is however not competitive with oxidative insertion due to a significantly higher barrier.

Yet, the novel S_N2-type dehydrogenation has a barrier that is essentially of the same height as that of the better-known stepwise dehydrogenation that proceeds via consecutive oxidative insertion and H migration from CH_3 to Pd. Therefore, the question arises whether such an S_N2-type mechanism might become feasible and active (besides the regular stepwise mechanism) in those reactions (see, for example, M^+ + CH_4)[16−18] in which dehydrogenation is know to occur.

Finally, for Pd + SiH_4 and the heavier congeners, there is only one TS for dehydrogenation. On the basis of the geometrical resemblance (especially for SiH_4) of this TS with the novel TS_{S_N2-ra}(C) found for Pd + CH_4, we have categorized the dehydrogenation pathway of the heavier substrates as the novel S_N2-type mechanism. We stress however that what happens in fact is a merging on the PES of the two saddle points TS_{S_N2-ra}(A) and $TS_{H-shift}$(A), and our categorization as S_N2-ra of the dehydrogenation mechanism for Pb + SiH_4, GeH_4, SnH_4, PbH_4 should thus not be overrated.

Acknowledgment. The authors would like to thank the Netherlands Organization for Scientific Research (NWO) for financial support.

Supporting Information Available: Additional energy and geometry data including Cartesian coordinates of all species occurring in this study. This material is available free of charge via the Internet at http://pubs.acs.org.

OM060274G